This manuscript was accepted by J. Chem. Phys. Click here to see the version of record.

Fluctuation effects in blends of A+B homopolymers with AB diblock copolymer

Russell K. W. Spencer* and Mark W. Matsen†

Department of Chemical Engineering,

Department of Physics & Astronomy,

and Waterloo Institute for Nanotechnology,

University of Waterloo, Waterloo, Ontario N2L 3G1, Canada

(Dated: April 30, 2018)

Abstract

Field-theoretic simulations (FTS) are performed on ternary blends of A- and B-type homopolymers of polymerization N_h and symmetric AB diblock copolymer of polymerization N_c. Unlike previous studies, our FTS are conducted in three-dimensional space, with the help of two new semi-grand canonical ensembles. Motivated by the first experiment to discover bicontinuous microemulsion (BμE) in the PE-PEP system, we consider molecules of high molecular weight with size ratios of $\alpha \equiv N_h/N_c = 0.1$, 0.2 and 0.4. Our focus is on the A+B coexistence between the two homopolymer-rich phases in the low-copolymer region of the phase diagram. The Scott line, at which the A+B phases mix to form a disordered (DIS) melt with increasing temperature (or decreasing χ), is accurately determined using finite-size scaling techniques. We also examine how the copolymer affects the interface between the A+B phases, reducing the interfacial tension towards zero. Although comparisons with self-consistent field theory (SCFT) illustrate that fluctuations effects are relatively small, fluctuations do nevertheless produce the observed BμE that is absent in the SCFT phase diagram. Furthermore, we find evidence of three-phase A+B+BμE coexistence, which may have been missed in the original as well as subsequent experiments.

This manuscript was accepted by J. Chem. Phys. Click here to see the version of record.

I. INTRODUCTION

AB diblock copolymers are known for their ability to compatiblize immiscible A+B homopolymers, in the same way surfactants cause water and oil to mix. The compatiblization results due to an accumulation of copolymer at the interfaces between the A- and B-rich phases,[1] which reduces the interfacial tension responsible for macrophase separation.[2] The potential for creating polymeric alloys has motivated a considerable amount of research. This has become particularly important in the recent quest to create sustainable materials endowed with properties that are competitive with traditional plastics and elastomers. The model system for these studies has been symmetric blends involving homopolymers of equal polymerization, N_h, and copolymers with two blocks of equal polymerization, $N_c/2$. Ideally, the A and B segments should have the same statistical length, a, in order to complete the symmetry. Note that we follow the convention where all segments are defined to have the same volume, ρ_0^{-1}.

Broseta and Fredrickson[3] classified the different behaviors of these ternary blends according to mean field theory. In the binary homopolymer limit, the disordered (DIS) melts macrophase separate to produce A+B coexistence at the critical point $(\chi N_h)_c = 2$, where χ is the usual Flory-Huggins parameter specifying the incompatibility of the unlike segments. As copolymer is added, the transition shifts to $(\chi N_h)_c = 2/(1-\bar{\phi}_c)$, where $\bar{\phi}_c$ is the volume fraction of copolymer. For size ratios of $\alpha \equiv N_h/N_c < 1$, the transition, referred to as the Scott line,[7] terminates in a Lifshitz critical point at $\bar{\phi}_{c,\mathrm{LP}} = 2\alpha^2/(1+2\alpha^2)$. Beyond that, the DIS phase transforms to a periodic lamellar (LAM) phase [see dotted curves in Fig. 1(b)].

Mean field theory or rather self-consistent field theory (SCFT), however, is only accurate in the infinite molecular-weight limit. The fluctuation corrections to it are controlled by the invariant polymerization indexes (e.g., $\bar{N}_h \equiv a^6\rho_0^2 N_h$). Although the corrections are generally small, they become significant near the order-disorder transition (ODT) causing a shift towards lower temperature (or higher χ). In the case of the Scott line, the fluctuations also change the critical exponents,[8,9] and in the case of the LAM/DIS boundary, they change the transition from continuous to discontinuous.[10,11] Fluctuations are expected to be particularly important near the Lifshitz point,[3,4] because of its large critical dimensions. The upper critical dimension, below which mean field theory becomes inaccurate, is eight as compared to four for the Scott line.[4] Furthermore, the lower critical dimension is believed to be four,[5,6]

which implies that the Lifshitz point should, in fact, be destroyed by fluctuations in three-dimensional space.

The critical behavior of the Lifshitz point was first investigated by Bates *et al.*[12] for blends of polyethylene (PE) and polyethylenepropylene (PEP) with $\alpha = 0.208$. (This choice of α roughly matches the ODT of neat diblock copolymer melts, $(\chi N_c)_{\rm ODT} \approx 10.5$, with the critical point of binary hompolymer blends, $(\chi N_h)_c \approx 2$, such that the ODT can be accessed over the full composition range, $0 \leq \bar{\phi}_c \leq 1$.) Bates *et al.* observed small-angle scattering consistent with a Lifshitz point exhibiting mean-field critical exponents to within 1°C of the apparent transition. Although the PE-PEP system should be well described by SCFT given the large $\bar{N}_h \approx 5000$,[13] Lifshitz points simply cannot exist in three dimensions. They suggested that fluctuations must, in reality, push the Lifshitz point to $T = 0$ leaving behind a channel of strongly-structured DIS phase, referred to as bicontinuous microemulsion (BμE) by the surfactant community.[14]

Two years later, Bates *et al.*[15] confirmed the proposed behavior [see Fig. 1(a)]. As expected, the position of the BμE channel corresponded well with the mean-field Lifshitz point, $\bar{\phi}_{c,\rm LP} = 0.080$. Subsequent experiments[16–23] have observed analogous behavior in a wide range of chemically different systems. These studies found stronger fluctuation effects for lower values of $\bar{N}_h$, in particular, a crossover towards the Lifshitz critical exponents[16,17] and a widening of the BμE channel.[18] It should be noted, however, that an increased width of the channel can also result from asymmetries in the system (i.e., mismatches in the homopolymer sizes, the copolymer blocks and/or the segment lengths),[19] which will exist to some extent in any real experimental system.

After Bates *et al.* proposed the BμE channel but before they actually discovered it, Müller and Schick[24] observed BμE in Monte Carlo (MC) simulations of the bond-fluctuation model. To avoid technical difficulties of conducting simulations in the grand canonical ensemble, they restricted their study to $\alpha = 1$, which allowed them to use a semi-grand canonical ensemble whereby polymers could switch among the different types. Computational costs also restricted their simulations to short polymers with $\bar{N}_h = 145$.[25] Not surprisingly, their phase diagram differed considerably from the experimental one, both quantitatively and qualitatively. In particular, their Scott line ended at an ordinary tricritical point, beyond which they found three-phase A+B+BμE coexistence followed by A+B+LAM coexistence.

Düchs *et al.*[26] later examined blends for $\alpha = 0.2$ using field-theoretic simulations (FTS),

FIG. 1: Phase diagrams for ternary blends obtained (a) experimentally[15] for PE-PEP with $\alpha = 0.208$ and (b) theoretically[27] from 2D FTS (symbols) and SCFT (dotted curves) with $\alpha = 0.2$. The diagrams include two-phase (A+B) coexistence, an ordered lamellar (LAM) phase and a disorder (DIS) phase, part of which is classified as bicontinuous microemulsion (BμE). The SCFT diagram also includes a narrow region of three-phase A+B+LAM coexistence (unlabeled) extending down from a Lifshitz critical point (solid dot). Note that the χN_h-axis of the simulation/theory diagram is inverted for easier comparison to the experimental one.

which do not suffer from the problems described above. They are ideally suited to handle large invariant polymerization indexes, and the grand canonical ensemble can be readily applied to any value of α. The FTS reproduced the channel of BμE separating the LAM phase from A+B coexistence, but showed no evidence of A+B+BμE coexistence. Subsequent FTS of the DIS phase also provided an approximate boundary separating the region of weakly-structured melts from that of BμE.[27] The resulting phase diagram is compared to the SCFT prediction in Fig. 1(b). It is important to note, however, that due to computational demands, these FTS were only performed in two-dimensional space. The authors acknowledged the limitation of 2D simulations, but that was the best they could do at the time.

Using recent developments in FTS[28,29] along with the introduction of two new semi-grand canonical ensembles, we perform the first simulations of symmetric A+B+AB blends in 3D. The simulations are performed for molecular size ratios of $\alpha \equiv N_h/N_c = 0.1, 0.2$ and 0.4 with experimentally-relevant sizes corresponding to $\bar{N}_h = 10^4$. The study focuses specifically on the compatiblization of the A+B homopolymers in the low-$\bar{\phi}_c$ region of the phase diagram, and results are directly compared to SCFT in order to assess the significance of fluctuation effects.

III. SIMULATION METHOD

This section describes field-theoretic simulations (FTS)[30,31] for an incompressible ternary blend of n_{hA} A-type homopolymers, n_{hB} B-type homopolymers and n_c AB diblock copolymers. The formalism is developed for symmetric blends, where all homopolymers have N_h segments and the diblocks are symmetric with $N_c/2$ segments in each block. Depending on the ensemble, we either set the homopolymer concentrations equal (i.e., $n_{hA} = n_{hB}$) or their chemical potentials equal. We also assume conformational symmetry, where A and B segments have the same statistical length, a. Thus, both homopolymers have the same unperturbed end-to-end length, $R_{0,h} = a\sqrt{N_h}$, which we use as our unit of length. Note that we follow the convention where all segments have the same volume, ρ_0^{-1}, such that the total volume of the system is $V = N_h(n_h + n_c/\alpha)/\rho_0$, where $n_h = n_{hA} + n_{hB}$ and $\alpha = N_h/N_c$. The volume fraction of diblock copolymer is $\bar{\phi}_c = n_c N_c/\rho_0 V$.

A. Single-chain partition functions

In FTS, the main computational task is to calculate the partition function, $Q_\gamma[W_-, W_+]$, for each molecular species ($\gamma = hA, hB$ and c) subjected to the external fields, $W_-(\mathbf{r})$ and $W_+(\mathbf{r})$, acting on the difference, $\hat{\phi}_-(\mathbf{r}) = \hat{\phi}_A(\mathbf{r}) - \hat{\phi}_B(\mathbf{r})$, and the total, $\hat{\phi}_+(\mathbf{r}) = \hat{\phi}_A(\mathbf{r}) + \hat{\phi}_B(\mathbf{r})$, of the A and B concentrations, respectively. To do this, we first parameterize the contour of the polymer by s, where $s = 0$ to 1 for the homopolymers and $s = 0$ to α^{-1} for the diblock copolymer. We then pin the s position of the polymer at $\mathbf{r}$, and calculate partial partition functions, $q_\gamma(\mathbf{r}, s)$ and $q_\gamma^\dagger(\mathbf{r}, s)$, for the small- and large-s parts of the molecule, using the standard Gaussian-chain model.[32] The first of these is obtained by solving the modified diffusion equation,

$$\frac{\partial q_\gamma}{\partial s} = \frac{R_{0,h}^2}{6}\nabla^2 q_\gamma - (W_- \pm W_+)q_\gamma \ , \tag{1}$$

forward in s starting from the initial condition $q_\gamma(\mathbf{r}, 0) = 1$. The '+' and '−' signs are used for the A and B portions of the molecule, respectively. The function $q_\gamma^\dagger(\mathbf{r}, s)$ is analogous to $q_\gamma(\mathbf{r}, s)$, but obtained by propagating from the other end of the molecule. Note that $q_\gamma^\dagger(\mathbf{r}, s) = q_\gamma(\mathbf{r}, 1-s)$ for homopolymer molecules. Once the partial partition functions have

This manuscript was accepted by J. Chem. Phys. Click here to see the version of record.

When calculated, the single-chain partition function for the entire molecule is given by

$$Q_\gamma[W_-, W_+] = \int q_\gamma(\mathbf{r}, s) q_\gamma^\dagger(\mathbf{r}, s) d\mathbf{r} \ , \tag{2}$$

where the integral can be evaluated for any value of s along the chain contour.

B. Total partition function

The Hamiltonian, $H[W_-, W_+]$, for FTS takes the simple form,[30]

$$\frac{N_h H}{k_B T \rho_0} = \frac{N_h H^Q}{k_B T \rho_0} + \int \left(\frac{W_-^2(\mathbf{r})}{\chi_b N_h} - W_+(\mathbf{r}) \right) d\mathbf{r} \ , \tag{3}$$

where H^Q is the free energy corresponding to a system of non-interacting molecules subjected to $W_-(\mathbf{r})$ and $W_+(\mathbf{r})$, and as such is expressed in terms of Q_γ. As in SCFT, H^Q is the only part of the Hamiltonian that depends on the type of ensemble. The Appendix outlines its derivation for the canonical (can) ensemble,[33]

$$\begin{aligned} \frac{N_h H^Q_{\text{can}}}{k_B T \rho_0 V} &= -\frac{1-\bar{\phi}_c}{2} \ln(Q_{hA}) - \frac{1-\bar{\phi}_c}{2} \ln(Q_{hB}) \\ &\quad -\alpha \bar{\phi}_c \ln(Q_c) \ , \end{aligned} \tag{4}$$

and for the grand canonical (gc) ensemble,[34]

$$\frac{N_h H^Q_{\text{gc}}}{k_B T \rho_0} = -Q_{hA} - Q_{hB} - z Q_c \ , \tag{5}$$

where $z = \exp(\mu / k_B T)$ is the fugacity and μ is the chemical potential of the copolymer relative to that of the homopolymers.

In addition to the standard canonical and grand canonical ensembles, the Appendix also derives H^Q for two new semi-grand canonical ensembles. The first (sgc1) allows n_{hA} and n_{hB} to fluctuate while constraining $n_h = n_{hA} + n_{hB}$ and n_c. Its Hamiltonian is given by

$$\frac{N_h H^Q_{\text{sgc1}}}{k_B T \rho_0 V} = -(1-\bar{\phi}_c) \ln(Q_{hA} + Q_{hB}) - \alpha \bar{\phi}_c \ln(Q_c) \ . \tag{6}$$

The second (sgc2) allows n_h and n_c to fluctuate under the constraint $n_{hA} = n_{hB}$. Its Hamiltonian is

$$\frac{N_h H^Q_{\text{sgc2}}}{k_B T \rho_0} = -2\sqrt{Q_{hA} Q_{hB}} - z Q_c \ . \tag{7}$$

This manuscript was accepted by J. Chem. Phys. Click here to see the version of record.

For a given Hamiltonian, $H[W_-, W_+]$, the partition function for the system,

$$Z \sim \int \exp\left(-\frac{H[W_-, W_+]}{k_B T}\right) \mathcal{D}W_- \mathcal{D}W_+ \ , \tag{8}$$

is obtained by performing functional integrals over the fields. To evaluate the energy per unit $k_B T$ in the Boltzmann weight, we need to multiply Eq. (3) by

$$\frac{\rho_0}{N_h} = \frac{\sqrt{\bar{N}_h}}{R_{0,h}^3} \ , \tag{9}$$

which is where the invariant polymerization index, $\bar{N}_h$, enters the FTS. All the simulations in this study are performed with $\bar{N}_h = 10^4$.

C. Saddle-point approximation

FTS are complicated by the fact that $W_+(\mathbf{r})$ is an imaginary-valued function, which in turn makes the Hamiltonian a complex-valued quantity. As a result, the Boltzmann weight, $\exp(-H/k_B T)$, is no longer positive definite, and therefore standard simulation methods are not applicable. Fredrickson and coworkers[30] have dealt with this by performing complex Langevin simulations (CL-FTS). We, instead, follow the strategy proposed by Schmid and coworkers,[26,27] whereby the functional integration over $W_+(\mathbf{r})$ in Eq. (8) is performed using the saddle-point approximation. This is done by evaluating $H[W_-, W_+]$ at its saddle-point with respect to $W_+(\mathrm{r})$, which we denote by $w_+(\mathbf{r})$. Fortunately, $w_+(\mathbf{r})$ turns out to be a real-valued function, which therefore permits standard Monte Carlo simulations (MC-FTS).

The saddle-point approximation enforces the incompressibility condition, $\hat{\phi}_+(\mathbf{r}) = 1$, in the mean-field approximation,

$$\phi_+(\mathbf{r}) \equiv \phi_{hA}(\mathbf{r}) + \phi_{hB}(\mathbf{r}) + \phi_c(\mathbf{r}) = 1 \ , \tag{10}$$

where

$$\phi_\gamma(\mathbf{r}) = C_\gamma \int q_\gamma(\mathbf{r}, s) q_\gamma^\dagger(\mathbf{r}, s) ds \tag{11}$$

is the average concentration of γ-type molecules in the system of non-interacting molecules.

This manuscript was accepted by J. Chem. Phys. Click here to see the version of record.

The coefficient for A-type homopolymer in the different ensembles is

$$C_{hA} = \begin{cases} \frac{(1-\bar{\phi}_c)V}{2Q_{hA}} , & \text{for can} , \\ 1 , & \text{for gc} , \\ \frac{(1-\bar{\phi}_c)V}{Q_{hA}+Q_{hB}} , & \text{for sgc1} , \\ \sqrt{\frac{Q_{hB}}{Q_{hA}}} , & \text{for sgc2} . \end{cases} \tag{12}$$

The analogous coefficient for B-type homopolymer, C_{hB}, is obtained by swapping the labels 'hA' and 'hB'. That of the copolymer is

$$C_c = \begin{cases} \frac{\alpha\bar{\phi}_c V}{Q_c} , & \text{for can} , \\ z , & \text{for gc} , \\ \frac{\alpha\bar{\phi}_c V}{Q_c} , & \text{for sgc1} , \\ z , & \text{for sgc2} . \end{cases} \tag{13}$$

Each time $W_-(\mathbf{r})$ is changed, we reevaluate $w_+(\mathbf{r})$ with Anderson mixing[36] such that

$$\left[\frac{1}{V}\int (\phi_+(\mathbf{r})-1)^2 d\mathbf{r}\right]^{1/2} < \epsilon . \tag{14}$$

One can readily show that the integrated concentrations are consistent with the different ensembles. For instance, $\int \phi_{hA}(\mathbf{r})d\mathbf{r} + \int \phi_{hB}(\mathbf{r})d\mathbf{r} = V(1-\bar{\phi}_c)$ in sgc1 and $\int \phi_{hA}(\mathbf{r})d\mathbf{r} = \int \phi_{hB}(\mathbf{r})d\mathbf{r}$ in sgc2, regardless of the fields. In particular, the total amount material is explicitly constrained in the canonical and first semi-grand canonical ensembles. As a result, $H[W_-, w_+]$ is unaffected by additive constants to $w_+(\mathbf{r})$, which allows us to fix its average value to zero. Furthermore, accurate results are obtained with a modest error tolerance of $\epsilon = 10^{-4}$. However, for the grand canonical and second semi-grand canonical ensembles, the amount of material is controlled by $w_+(\mathbf{r})$ and a higher error tolerance of $\epsilon = 10^{-7}$ is required to achieve similar accuracy.

D. Ultraviolet divergence

The FTS are performed in simulation boxes with sides of lengths L_x, L_y and L_z (i.e., $V = L_x L_y L_z$). We generally apply periodic boundary conditions, but for the purposes of creating a single A/B interface we also make use of reflecting boundary conditions. For computational purposes, the fields, $W_-(\mathbf{r})$ and $w_+(\mathbf{r})$, are defined on a discrete grid with uniform spacings of Δ_x, Δ_y and Δ_z in the three respective directions. One might expect results to converge as $\Delta_\nu \to 0$, but instead they exhibit an ultraviolet (UV) divergence.[37] Fortunately, for polymers of high molecular weight, this divergence can be removed by expressing results in terms of an effective Flory-Huggins χ parameter, defined by

$$\frac{\chi}{\chi_b} = 1 - \frac{12 R_{0,h}}{\pi^3 \sqrt{\bar{N}_h}} \int_0^{\Lambda_z} \int_0^{\Lambda_y} \int_0^{\Lambda_x} \frac{dk_x dk_y dk_z}{k_x^2 + k_y^2 + k_z^2} \ , \tag{15}$$

where $\Lambda_\nu = \pi/\Delta_\nu$ is the wavevector cutoff in the ν-direction. Here, we choose equal grid spacings, Δ, for all three dimensions, in which case[28]

$$\frac{\chi}{\chi_b} = 1 - \frac{2.333}{\sqrt{\bar{N}_h}} \frac{R_{0,h}}{\Delta} \ . \tag{16}$$

Note that our simulations are all performed with the same resolution of $\Delta = 0.375 R_{0,h}$, for which $\chi = 0.938 \chi_b$.

E. Monte Carlo algorithm

Each Monte Carlo step (MCS) involves making a small change to $W_-(\mathbf{r})$, followed by the reevaluation of $w_+(\mathbf{r})$. The moves are accepted or rejected based on the standard Metropolis criterion. For the canonical and second semi-grand canonical ensembles, we alternate between two kinds of moves: one in real space where $W_-(\mathbf{r})$ is changed at each grid point by amounts selected from a uniform distribution, and another in Fourier space where $W_-(\mathbf{k})$ is changed at each wavevector with a probability proportional to the RPA structure function, $S_{\mathrm{RPA}}(\mathbf{k})$, corresponding to a binary homopolymer blend of $\chi N_h = 1.8$. For the grand canonical and first semi-grand canonical ensembles, we include a third move that changes $W_-(\mathbf{r})$ by a constant chosen from a uniform distribution. The amplitude of each move is adjusted during the beginning of the equilibration period to achieve an acceptance rate of $\sim 40\%$. We typically use 10^5 MCS to equilibrate the system, followed by $10^6 - 10^7$ MCS for the collection of statistics. Observables are sampled once every 40 MCS.

This manuscript was accepted by J. Chem. Phys. Click here to see the version of record.

In order to save computational effort in locating the Scott line, we use Monte Carlo reweighting[38,39] to determine the $\chi_b N_h$-dependence of an observable, $\hat{O}$. This is done by conducting a single simulation at a particular $(\chi_b N_h)^*$, and storing the values of $\hat{O}$ as well as

$$\hat{I} \equiv \int W_-^2(\mathbf{r}) d\mathbf{r} \tag{17}$$

over m configurations of the system.[29] The ensemble average of $\hat{O}$ at $\chi_b N_h$ is then given by

$$\langle \hat{O} \rangle = \frac{1}{\mathcal{N}} \sum_{i=1}^{m} \hat{O}_i \exp\left(\frac{\rho_0}{N_h} \left[\frac{1}{(\chi_b N_h)^*} - \frac{1}{\chi_b N_h} \right] \hat{I}_i \right), \tag{18}$$

where the normalization constant is[40]

$$\mathcal{N} = \sum_{i=1}^{m} \exp\left(\frac{\rho_0}{N_h} \left[\frac{1}{(\chi_b N_h)^*} - \frac{1}{\chi_b N_h} \right] \hat{I}_i \right). \tag{19}$$

Naturally, the accuracy of the reweighting decreases as $\chi_b N_h$ deviates from $(\chi_b N_h)^*$. However, the range of applicability is large near critical points (e.g., the Scott line), due to the fact that critical fluctuations create a broad distribution of configurations.

III. RESULTS

In this study, we focus on the two-phase A+B region in Fig. 1. Our calculations are all performed for homopolymers of invariant polymerization index $\bar{N}_h = 10^4$, which roughly matches the experiments of Bates *et al.*[12,13,15] Although the experiments were only for $\alpha \equiv N_h/N_c \approx 0.2$, we consider three different copolymer sizes corresponding to $\alpha = 0.1$, 0.2 and 0.4.

A. Scott line

Our first task is to locate the Scott line separating A+B coexistence from the mixed DIS state. The natural order parameter for this critical transition is the difference in the total number of A and B segments, $\bar{\phi}_- = V^{-1} \int \hat{\phi}_-(\mathbf{r}) d\mathbf{r}$. The 2D simulations of Düchs *et al.*[26,27] estimated the transition, $(\chi N_h)_c$, by simply looking for the point of broken symmetry (i.e., $\langle \bar{\phi}_- \rangle \neq 0$) in a grand canonical simulation. We instead employ a far more accurate finite-scaling method,[41] which identifies the transition by the fixed point where the fourth-order

FIG. 2: Fourth-order cumulant, U_L, plotted for system sizes of $L/R_{0,h} = 2.25$ (solid), 3.0 (dots), 4.125 (dashes) and 5.25 (dot-dot-dashes). Results are shown for compositions of $\bar{\phi}_c = 0.00$, 0.02 and 0.04 at copolymer sizes corresponding to (a) $\alpha = 0.1$, (b) $\alpha = 0.2$ and (c) $\alpha = 0.4$.

cumulant,

$$U_L = 1 - \frac{\langle \bar{\phi}_-^4 \rangle}{3\langle \bar{\phi}_-^2 \rangle^2}, \tag{20}$$

becomes independent of system size, L. The moments of $\bar{\phi}_-$ are related to moments of $\bar{W}_-$ by expressions derived in Ref. 29, where we applied the method to binary homopolymer blends. That study used the grand canonical ensemble, but this time we use the semi-grand canonical (sgc1) ensemble in Eq. (6), which proves to be far more stable and accurate.

The fixed point is determined by plotting U_L as a function of χN_h for different system sizes, L, as illustrated in Fig. 3 for various combinations of $\bar{\phi}_c$ and α. To save computational effort, the χN_h-dependence was determined by MC reweighting of simulations performed at $(\chi N_h)^* = 2.0125$, 2.065 and 2.125 for $\bar{\phi}_c = 0.00$, 0.02 and 0.04, respectively. Apart from one exception that will be discussed shortly, the curves from the different system sizes cross at a common point, which identifies $(\chi N_h)_c$. Furthermore, the cumulants collapse when the axes are scaled with the system size using the 3D-Ising exponent $\nu = 0.62997$, as demonstrated previously in Ref. 29. In fact, the collapse is improved now that we are using the sgc1 ensemble.

Figure 3 compares the critical points from all our FTS to the mean-field prediction, $(\chi N_h)_c = 2/(1 - \bar{\phi}_c)$. Note that there are three independent results from Fig. 2 corresponding to binary homopolymer blends (i.e, $\phi_c = 0$). The slight variation in these results, which is entirely due to statistical noise, proves to be relatively small. Furthermore, these results agree well with the universal prediction $(\chi N_h)_c \approx 2 + 1.5\bar{N}_h^{-1/2} = 2.015$ for binary blends.[9] Interestingly, the fluctuation correction to mean-field theory increases considerably as copolymer is added to the system. Nevertheless, the Scott line remains independent of the copolymer size, α, to within our statistical accuracy. As discussed previously,[3,7] this

FIG. 3: Critical points, $(\chi N_h)_c$, calculated along the Scott line for $\alpha = 0.1$ (triangles), $\alpha = 0.2$ (circles) and $\alpha = 0.4$ (squares). The solid curve denotes the mean-field prediction of the Scott line, and the crosses mark the mean-field Lifshitz points for $\alpha = 0.1$ and 0.2; the Lifshitz point for $\alpha = 0.4$ lies beyond the range of the plot.

FIG. 4: Typical configurations [i.e., density plots of $W_-(\mathbf{r})$] along the Scott line at $\bar{\phi}_c = 0.04$ and $\chi N_h = 2.1$ for copolymer sizes corresponding to (a) $\alpha = 0.1$, (b) $\alpha = 0.2$ and (c) $\alpha = 0.4$. The size of the simulation box is $L = 5.25R_{0,h}$.

independence provides confirmation that the effect of copolymer on $(\chi N_h)_c$ is primarily entropic.

The failure of the finite-size scaling, which we eluded to above, occurred for $\alpha = 0.1$ and $\bar{\phi}_c = 0.04$ in Fig. 2(a). While the cumulants for the two smaller system sizes cross at the expected location, $(\chi N_h)_c \approx 2.10$, consistent with a Scott line that is independent of α, the cumulants for the larger two systems deviate from this expectation. To help understand why, Fig. 4 compares sample configurations from the largest $L = 5.25R_{0,h}$ simulation box at $\bar{\phi}_c = 0.04$ and $\chi N_h = 2.1$ for the three different values of α. The configurations for $\alpha = 0.2$ and 0.4 exhibit relatively modest fluctuations, whereas the configuration for $\alpha = 0.1$ resembles a strongly-segregated microemulsion-like morphology. Naturally, the occurrence of this morphology is only possible when the simulation box is sufficiently large relative to its domain size, which explains why the cumulants for the two smaller systems remain consistent with a critical point at $\chi N_h \approx 2.1$.

The anomalous behavior of the cumulants implies that we have overrun the end of the Scott line, which contradicts the suggestion by Fig. 1 that the Scott line extends to $T = 0$.

FIG. 5: Adsorption isotherms for (a) different segregations at $\alpha = 0.2$ and (b) different copolymer sizes at $\chi N_h = 3$. Solid curves denote SCFT predictions, and the slope of one at small $\bar{\phi}_c$ confirms the relationship in Eq. (21).

On the otherhand, this is somewhat consistent with the mean-field prediction that it terminates at $\bar{\phi}_{c,\mathrm{LP}} = 0.0196$ for $\alpha = 0.1$. The observation of BμE-type configurations like that of Fig. 4(a) suggests that the Scott line ends at an ordinary tricritical point followed by A+B+BμE coexistence, rather than a Lifshitz critical point followed by A+B+LAM coexistence as predicted by SCFT.[3,27] In principle, a finite-size scaling analysis could locate the tricritical point, but it would require much larger systems sizes and exceptionally accurate statistics,[42] which is beyond the scope of this paper. In any case, we will encounter more compelling evidence for A+B+BμE coexistence in the next section.

B. Adsorption Isotherms

For the remainder of this paper, the bulk copolymer concentration, $\bar{\phi}_c$, will be controlled by adjusting the chemical potential, μ. Figure 5 shows some adsorption isotherms, which allows one to convert between μ and $\bar{\phi}_c$. They are evaluated in the grand canonical ensemble by increasing μ in small increments, equilibrating and then collecting statistics for $\bar{\phi}_c$. The FTS results agree well with SCFT (solid curves), which implies that fluctuation effects are relatively small at these low copolymer concentrations. Note that the concentrations are plotted on a logarithmic scale in order to demonstrate the dependence,[24]

$$\bar{\phi}_c \propto \exp(\mu/k_B T) \ , \tag{21}$$

which proves to be accurate for this limited range of $\bar{\phi}_c$.

On closer examination of Fig. 5(a), we see that the copolymer concentration in the A+B coexistence region (i.e., $\chi N_h \gtrsim 2.015$) begins to increase more rapidly with μ at $\bar{\phi}_c \sim 0.1$. Figure 6 extends the plots for $\chi N_h = 2.4$ and 3.0 to larger μ, revealing a

FIG. 6: Adsorption isotherms calculated for $\alpha = 0.2$ with (a) $\chi N_h = 2.4$ and (b) $\chi N_h = 3.0$. The dots and crosses are from simulations where μ is incremented in the positive and negative directions, respectively. The hysteresis loops imply phase coexistence, while the representative configurations taken from the upper and lower branches (insets) indicate A+B+BμE coexistence.

sudden jump in $\bar{\phi}_c$ similar to what was observed by Müller and Schick.[24] Interestingly, combining the data obtained by increasing μ (solid dots) with equivalent data obtained by decreasing μ (crosses) produces well-defined hysteresis loops, which implies the existence of a discontinuous phase transition. The insets show sample configurations from the low- and high-copolymer branches of the adsorption isotherms, which provides compelling evidence that the phase transition corresponds to three-phase A+B+BμE coexistence.

Although the phase transition must occur somewhere within the hysteresis loops, we cannot say exactly where. The hysteresis loops could be narrowed by equilibrating the system for more MCS at each value of μ, but not sufficiently to obtain the transition accurately. This could be accomplished by using, for example, thermodynamic integration[43,44] or a Gibbs ensemble.[45] However, the simulation boxes would have to be considerably larger than the domain size of the BμE phase to avoid significant finite-size effects. Nevertheless, the particle-based simulations of Müller and Schick[24] suggest that the transition can be estimated by the point where the interfacial tension, σ, between the two homopolymer-rich phases becomes zero. As we show in the next section, $\sigma \to 0$ at $\mu/k_BT \approx 1.4$ for $\chi N_h = 3$, which implies that the binodals of the A+B+BμE region are $\bar{\phi}_c \approx 0.02$ and 0.16. Note that this estimated width is considerably larger than that of the A+B+LAM region predicted by SCFT.[27]

C. A/B interface

Our attention now turns to the A/B interface between the coexisting A+B phases. For this, we use the second semi-grand canonical (sgc2) ensemble, which balances the amount

FIG. 7: A-segment (circles) and copolymer (crosses) concentration profiles plotted across an A/B interface at $\chi N_h = 3.0$ for (a) $\alpha = 0.1$, (b) $\alpha = 0.2$ and (c) $\alpha = 0.4$. Note that the simulation boxes extend well beyond the range of the plots. Solid curves denote SCFT predictions.

of A- and B-type homopolymers while allowing the total amount of homopolymer (and thus copolymer) to fluctuate. To create a single interface perpendicular to the x-axis, we switch the boundary condition in the x-direction from periodic to reflecting and use a simulation box with $L_x > L_y = L_z$. Balancing the amount of homopolymers constrains the interface to the center of the box (defined as $x = 0$), and allowing the amount of copolymer to fluctuate reduces finite-size effects.

Although the concentrations, $\phi_\gamma(\mathbf{r})$, obtained from the propagators in Eq. (11) have no physical meaning in FTS, their ensemble averages are equal to those of the instantaneous concentrations, $\hat{\phi}_\gamma(\mathbf{r})$.[30,46] Using this fact, we evaluate the copolymer profile, $\langle\hat{\phi}_c(x)\rangle$, across the A/B interface by spatially averaging $\phi_c(\mathbf{r})$ over y and z and then ensemble averaging over a simulation. Similarly, the A-segment concentration, $\langle\hat{\phi}_\mathrm{A}(x)\rangle$, is obtained by averaging $\phi_{h\mathrm{A}}(\mathbf{r}) + \phi_{c\mathrm{A}}(\mathbf{r})$, where $\phi_{c\mathrm{A}}(\mathbf{r})$ is given by Eq. (11) with the s-integration performed over the A block.

The copolymer (crosses) and A-segment (circles) concentration profiles are shown in Fig. 7 at $\chi N_h = 3$ for different copolymer sizes, α. Note that the length of the simulation box is chosen large enough ($L_x = 18R_{0,h}$ for $\alpha = 0.1$ and $L_x = 9R_{0,h}$ for $\alpha = 0.2$ and 0.4) to reach bulk concentrations at the edges. The FTS results all agree reasonably well with SCFT (solid curves), indicating that fluctuation effects are relatively minor.

The excess copolymer concentration, $\langle\hat{\phi}_c(x)\rangle - \bar{\phi}_c$, is reasonably narrow for $\alpha = 0.2$ and 0.4, which is indicative of the mushroom regime where the copolymers remain relatively unstretched. In contrast, the profile is much wider for $\alpha = 0.1$, indicating that the copolymer blocks are forming stretched brushes, albeit wet brushes given that the maximum copolymer concentration is only about 20%.

The A-segment concentration fits well to the usual sigmodial profile,

FIG. 8: Interfacial width, w_I, calculated at $\chi N_h = 3$ for $\alpha = 0.1$ (triangles), $\alpha = 0.2$ (circles) and $\alpha = 0.4$ (squares). Solid curves denote SCFT predictions.

FIG. 9: Interfacial tension, σ, calculated at $\chi N_h = 3$ for $\alpha = 0.1$ (triangles), $\alpha = 0.2$ (circles) and $\alpha = 0.4$ (squares). Solid curves denote SCFT predictions

$\langle \phi_A(x) \rangle \propto [\tanh(2x/w_I) + 1]$, where the fitting parameter w_I represents the interfacial width. Figure 8 plots the change in w_I for $\chi N_h = 3$ as copolymers of different sizes are added to the blend. The largest copolymer ($\alpha = 0.1$) causes a modest narrowing of the interface implying an enhancement in segregation, while the shorter copolymers ($\alpha = 0.2$ and 0.4) have the opposite effect. The SCFT predictions (solid curves) agree well with the FTS. We might have expected some broadening of the interface relative to the SCFT predictions due to capillary-wave fluctuations,[42,47] but we see no evidence of this. This is undoubtedly because the fluctuations are suppressed as a result of the relatively small lateral dimensions, $L_y = L_z = 3R_{0,h}$, of our simulation boxes. It should be feasible to extend our FTS to systems of sufficient size to study the capillary waves, but that is beyond the scope of this initial study.

The free energy of the coexisting A+B phases has the form $F = f_{\rm bulk} V + \sigma A$, where $f_{\rm bulk}$ is free energy density in the bulk, σ is the A/B interfacial tension, $V = L_x L_y L_z$ is the volume of the system and $A = V/L_x$ is the area of the interface. From this, it immediate follows that

$$\sigma = -\frac{L_x^2}{V}\frac{\partial F}{\partial L_x} = \frac{L_x^2}{k_B T V}\left\langle \frac{\partial H_{\rm sgc2}}{\partial L_x} \right\rangle , \qquad (22)$$

where the derivative with respect to L_x is performed at constant volume.[48,49] In FTS, the

FIG. 10: Test of the Gibbs adsorption isotherm, Eq. (24), for $\alpha = 0.1$ (triangles), $\alpha = 0.2$ (circles) and $\alpha = 0.4$ (squares). The left and right sides of the equation are plotted with open and closed symbols, respectively. Solid curves denote SCFT predictions.

derivate of the Hamiltonian has a nice analytical expression,

$$\frac{N_h}{k_B T \rho_0}\frac{\partial H_{\rm sgc2}}{\partial L_x} = -\sqrt{\frac{Q_{hB}}{Q_{hA}}}\frac{\partial Q_{hA}}{\partial L_x} - \sqrt{\frac{Q_{hA}}{Q_{hB}}}\frac{\partial Q_{hB}}{\partial L_x} - z\frac{\partial Q_c}{\partial L_x} \ , \tag{23}$$

in terms of derivatives of Q_γ, which in turn have analytical expressions provided in Refs. 44 and 45. Normally, a change in L_x at constant V would have to be accompanied by a change in χ_b, so as to keep the effective χ constant. Thus, Eq. (23) would, in general, require an additional term proportional to the derivative $\partial\chi_b/\partial L_x$.[44] However, this derivative becomes zero when the grid resolution, Δ_ν, is the same in all three dimensions.

Figure 9 plots the interfacial tension, σ, at $\chi N_h = 3$ for our three different copolymer sizes, α. As expected, the addition of copolymer drives the tension towards zero. Referring to Fig. 5(b), the tension becomes zero at $\bar{\phi}_c \approx 0.15$, 0.020 and 0.0001 for $\alpha = 0.4$, 0.2 and 0.1, respectively, consistent with the understanding that longer copolymers have a stronger compatibilzation power.[3] Again, the FTS results agree well with SCFT (solid curves). The most significant difference is in the binary limit (i.e., $\bar{\phi}_c = 0$), where the SCFT underestimates the tension by about 10%. Naturally, our FTS values of σ will be affected by the suppression of capillary waves, but previous simulations have shown the effect to be very small.[50]

We conclude our study by checking the accuracy of our FTS in regards to the Gibbs adsorption isotherm,[1,24]

$$\Theta_c = -N_c\frac{d\sigma}{d\mu} \ , \tag{24}$$

which relates the copolymer excess,

$$\Theta_c \equiv \rho_0 \int (\langle \phi_c(x) \rangle - \bar{\phi}_c) dx \ , \tag{25}$$

obtained from Fig. 7 to the rate the surface tension changes in Fig. 8. To reduce statistical noise, the value of $d\sigma/d\mu$ at a given value of μ is obtained from a quadratic fit to the data point at μ plus the three data points to either side. The copolymer excess (solid symbols) and the derivate of the surface tension (open symbols) are compared in Fig. 10 at $\chi N_h = 3$ for the three different values of α. The agreement is significantly better than that obtained in the particle-based simulations of Müller and Schick,[24] because we are employing an incompressible model. In fact, the SCFT results (solid curves) are found to satisfy Eq. (24) perfectly. As before, SCFT agrees well with our FTS, reconfirming that fluctuation effects on the A/B interface are negligible at $\bar{N}_h = 10^4$.

IV. DISCUSSION

With the help of increased computation power, improved numerical algorithms[51,52] and two new ensembles, we have extended the previous FTS of ternary A+B+AB blends[26,27] from 2D to 3D. In standard particle-based simulations, changing the dimensionality affects the number of intermolecular contacts, which in turn impacts the level of fluctuations. Fortunately, the chain concentration (i.e., ρ_0/N_h) is one of the control parameters in FTS, and so this effect can be partially accounted for in 2D simulations. However, the details of critical transitions (e.g., their critical exponents) will nevertheless be affected by the dimensionality of the system. Furthermore, dimensionality will also affect the modes available to a fluctuating A/B interface in, for example, the BμE morphology. Thus, the only way to obtain quantitatively reliable results is to perform simulations in the appropriate dimension.

Although our MF-FTS account for fluctuations in the composition field, $W_-(\mathbf{r})$, they still invoke the saddle-point approximation for the pressure field, $W_+(\mathbf{r})$. In principle, this approximation could be removed by performing CL-FTS.[30,31] Nevertheless, the $W_-(\mathbf{r})$ fluctuations are expected to provide the dominant correction to SCFT, and thus the approximation for $W_+(\mathbf{r})$ should be relatively accurate. Indeed, the MC-FTS and CL-FTS results of the 2D simulations in Ref. 26 were indistinguishable. It is also worth noting that the MC-FTS in that study coped far better with the large fluctuations near the microemulsion region of

ing phase diagram.

Our choice of invariant polymerization index, $\bar{N}_h = 10^4$, roughly matches the PE-PEP system studied by Bates *et al.*[12,13,15] Given this large value, fluctuation effects would normally be very small. Indeed, the properties of the A/B interface are almost indistinguishable from the SCFT predictions. However, Fig. 3 demonstrates that the fluctuation correction to the Scott line becomes substantial as copolymer is added. This then leads to the most notable correction, which is the qualitative change at the end-point of the Scott line. Our observation of A+B+BμE implies that the Lifshitz critical point predicted by mean field theory is replaced by an ordinary tricritical point. In reality, the Lifshitz point was certain to be destroyed by fluctuations given that its lower critical dimension is greater than three. Its replacement by an ordinary critical point is consistent with the particle-based simulations of Müller and Schick for $\alpha = 1$ and $\bar{N}_h = 145$.[24]

Although experiments have observed A+B+BμE coexistence in blends with $\alpha \approx 1$,[2,53] there has yet to be any experimental evidence of it for $\alpha \approx 0.2$.[15–23] We suspect that the experiments observed swollen BμE in place of the more stable three-phase coexistence. The problem is that the attraction between A/B interfaces, which would be responsible for a swollen BμE phase shedding excess homopolymer, is extraordinarily weak.[54] The large hysteresis loops in Fig. 6 can be attributed to the same issue. Nevertheless, it might still be possible to observe A+B+BμE in experiments by allowing substantially long annealing times.

Previous particle-based simulations for the Scott line[24] and the A/B interface[50] also compared their results to SCFT. However, these comparisons are not as definitive as ours, due to ambiguities in defining an effective χ for particle-based simulations.[9,11,25] Likewise, the same issue exists for previous experimental comparisons to SCFT.[1,2] On the other hand, we have a clear relationship between the bare interaction parameter χ_b used in FTS and the effective χ that should be used when comparing to SCFT.[28,29] We note, though, that the ambiguity in defining χ seems to have now been resolved for particle-based simulations[11] as well as experiments.[55]

FTS have various advantages over particle-based simulations. For instance, there is the option of reflecting boundary conditions as used in our simulation of the A/B interface. In the particle-based simulations of Müller and coworkers,[24,50] the A/B interface was created by confining the melt between hard walls that favored A- and B-type monomers. Naturally,

hard walls cause a considerable disruption in the bulk behavior. Admittedly, reflecting boundaries do as well given that they restrict the possible composition fluctuations, but the level of disruption is certainly far less.

In particle-based simulations, it is difficult to find space in the simulation box for the insertion of new molecules, particularly for large polymers, which renders the grand canonical ensemble problematic. Müller and Schick[24] circumvented this problem by setting the polymerization of all their molecules to $N = 32$. That allowed them to employ a semi-grand canonical ensemble, whereby molecules were able to swap between the three species by a simple relabeling of the monomer types. Of course, this restricted their study to $\alpha = 1$. In principle, the approach can be extended to blends, in which the ratios of polymerizations are all integers, by cutting or joining together polymers as they switch identity.[56] However, the computational cost becomes extraordinary for ratios greater than three. These issues render particle-based simulations for $\alpha = 0.1$, 0.2 and 0.4 impractical.

In FTS, there is no inherent problem with employing the grand canonical ensemble, but nevertheless the semi-grand canonical ensembles have significant advantages. The sgc1 ensemble explicitly constrains the total amount of material in the system, whereas the grand canonical ensemble has to control the amount of material using $w_+(\mathbf{r})$. The explicit constraint increases the speed and stability of the Anderson-mixing algorithm. The sgc2 ensemble has the advantage that it constrains the position of the A/B interface, whereas it is free to drift in the grand canonical ensemble. These type of advantages could also be useful in SCFT calculations.

We have presented our semi-grand ensembles for symmetric blends, but they can be generalized to asymmetric compositions. A chemical potential difference, μ_ψ, between the homopolymers can be incorporated into the sgc1 ensemble by generalizing the Hamiltonian to

$$\begin{aligned}\frac{N_h H^Q_{\text{sgc1}}}{k_B T \rho_0 V} &= -(1-\bar{\phi}_c)\ln(z_\psi^{1/2} Q_{hA} + z_\psi^{-1/2} Q_{hB}) \\ &\quad -\alpha\bar{\phi}_c \ln(Q_c)\ , \end{aligned} \tag{26}$$

where $z_\psi = \exp(\mu_\psi/k_BT)$. Likewise, the Hamiltonian of the sgc2 ensemble can be generalized to

$$\frac{N_h H^Q_{\text{sgc2}}}{k_B T \rho_0} = -\left(\frac{Q_{hA}}{\psi}\right)^{\psi}\left(\frac{Q_{hB}}{1-\psi}\right)^{(1-\psi)} - zQ_c\ , \tag{27}$$

allow for an asymmetric amount, $\psi = n_{hA}/n_h$, of A-type homopolymer. Although the ensembles can handle asymmetric compositions, they are nevertheless limited to the special case of $N_{hA} = N_{hB}$. The restriction is because the factorials, $n_{hA}!$ and $n_{hB}!$, accounting for the indistinguishability of like molecules in the partition function must have an appropriate form so that the sums over n_{hA} and n_{hB} result in closed-form expressions (see Appendix).

V. SUMMARY

The compatibilization of immiscible A+B homopolymers of equal size N_h by symmetric AB diblock copolymers of size N_c was investigated with three-dimensional (3D) field-theoretic simulations (FTS). The incompressibility of the melt was enforced within the mean-field approximation, which allowed us to apply standard Monte Carlo techniques. Motivated by the experiments of Bates *et al.*,[15] we considered molecular sizes corresponding to $\alpha \equiv N_h/N_c = 0.1$, 0.2 and 0.4 with an invariant polymerization index of $\bar{N}_h \equiv a^6\rho_0^2 N_h = 10^4$. The focus of our study was on the Scott line in Fig. 1 and the interface between coexisting A+B homopolymer-rich phases. By comparing our FTS results to self-consistent field theory (SCFT), we were able to access the level of fluctuation effects, as controlled by the value of $\bar{N}_h$.

The simulations of the A/B interface examined the A-segment profile $\langle\hat{\phi}_A(\mathbf{r})\rangle$, the copolymer profile $\langle\hat{\phi}_c(\mathbf{r})\rangle$, the interfacial width w_I, the interfacial tension σ and the copolymer excess Θ_c. In all cases, the FTS results agreed well with SCFT, implying that fluctuation effects on the A/B interface are negligible at $\bar{N}_h = 10^4$. Admittedly, capillary-wave fluctuations were suppressed in our FTS due to the limited size of the simulation boxes, and thus it would be useful to conduct further FTS analogous to the particle-based simulations of Werner *et al.*[50]

The Scott line exhibited a more significant deviation from the SCFT prediction, $(\chi N_h)_c = 2/(1-\bar{\phi}_c)$.[3] Although it continued to show no dependence on α, fluctuations did cause a significant shift towards higher χN_h (i.e., lower temperature) that grew in size with the addition of copolymer. The most notable deviation from SCFT was the appearance of three-phase coexistence between the A+B homopolymer-rich phases and a bicontinuous microemulsion (BμE). This implies that the Scott line terminates at an ordinary tricritical point as opposed to a Lifshitz critical point.[24] Although the metastability of the competing

phases prevented a precise determination of the binodals, it was nevertheless clear that the A+B+BμE region in Fig. 1(a) is relatively wide. It may have been missed in the experiments due to insufficient annealing times on account of the high degrees of metastability.

Our application of FTS to 3D was greatly aided by two new semi-grand canonical ensembles. The first allowed the numbers of A and B homopolymers, n_{hA} and n_{nB}, to fluctuate while constraining the total $n_h = n_{hA} + n_{hB}$. This greatly improved the numerical efficiency and stability in calculating the fourth-order cumulant, U_L, used to locate the Scott line, in comparison to the previous use of the grand canonical ensemble.[29] The second permitted n_h to fluctuate under the constraint $n_{hA} = n_{hB}$. This combined with the ability of FTS to impose reflecting boundaries helped simulate A/B interfaces. Furthermore, the ability of calculating changes in free energy with respect to variations in the dimensions of the simulation box gave direct access to the surface tension. Further advantages of FTS over traditional particle-based simulations will undoubtedly emerge as this new approach receives more attention.

ACKNOWLEDGMENTS

We are grateful to Frank Bates for valuable discussions. This work was funded through a collaboration with the University of Minnesota's Center for Sustainable Polymers (CHE-1413862). Calculations were performed using the SHARCNET facility of Compute Canada.

APPENDIX A: HAMILTONIANS FOR VARIOUS ENSEMBLES

The only part of the field-theoretic Hamiltonian, Eq. (3), that depends on the type of ensemble is H^Q, the free energy of non-interacting polymers subjected to the external fields, $W_-(\mathbf{r})$ and $W_+(\mathbf{r})$. In the canonical (can) ensemble, where the number of molecules, n_γ, of each polymer species, γ, is fixed,[33]

$$\frac{H^Q_{\rm can}}{k_BT} = -\ln\left(\frac{Q_{hA}^{n_{hA}}Q_{hB}^{n_{hB}}Q_c^{n_c}}{n_{hA}!n_{hB}!n_c!}\right) \ . \tag{A1}$$

The Q_γ's are the partition functions for single molecules and the factorials account for the indistinguishability of identical molecules. Given that the n_γ's are fixed, the factorials simply add a constant to $H^Q_{\rm can}$ and therefore can be ignored. Dropping them and using the fact

that $n_{hA} = n_{hB} = (1 - \bar{\phi}_c)\rho_0 V/2N_h$ and $n_c = \alpha\bar{\phi}_c\rho_0 V/N_h$ leads directly to the expression in Eq. (4).

In the grand canonical (gc) ensemble, we include $z = \exp(\mu/k_BT)$ to control the copolymer concentration and sum over all possible numbers of molecules, which gives[34]

$$\frac{H^Q_{\rm gc}}{k_BT} = -\ln\left(\sum_{n_{hA}=0}^{\infty}\sum_{n_{hB}=0}^{\infty}\sum_{n_c=0}^{\infty}\frac{Q_{hA}^{n_{hA}}Q_{hB}^{n_{hB}}(zQ_c)^{n_c}}{n_{hA}!n_{hB}!n_c!}\right) . \tag{A2}$$

Note that we are effectively setting both homopolymer chemical potentials equal to zero, which maintains the symmetry of the blend. Without loss of generality, we can multiply each Q_γ by a factor of ρ_0/N_h, which adds an irrelevant constant to all the chemical potentials. Given the identity $e^x = \sum_n x^n/n!$, Eq. (5) immediately follows.

In our first semi-grand canonical (sgc1) ensemble, the numbers of A and B homopolymers are allowed to fluctuate, while the total number $n_h = n_{hA} + n_{hB}$ is held fixed. In this case, the Hamiltonian becomes

$$\begin{aligned}\frac{H^Q_{\rm sgc1}}{k_BT} &= -\ln\left(\sum_{n_{hA}=0}^{n_h}\frac{Q_{hA}^{n_{hA}}Q_{hB}^{n_h-n_{hA}}Q_c^{n_c}}{n_{hA}!(n_h-n_{hA})!n_c!}\right) ,\\ &= -\ln\left(\frac{(Q_{hA}+Q_{hB})^{n_h}Q_c^{n_c}}{n_h!n_c!}\right) .\end{aligned} \tag{A3}$$

Note that the sum is evaluated using the Binomial theorem, $(x+y)^m = \sum_n C_m^n x^n y^{(m-n)}$, where $C_m^n = m!/n!(m-n)!$ Using the fact $n_h = (1-\bar{\phi}_c)\rho_0 V/N_h$ and dropping additive constants, we obtain Eq. (6).

In the second semi-grand canonical (sgc2) ensemble, we constrain $n_{hA} = n_{hB} = n_h/2$. In cases of odd n_h, the numbers of A and B homopolymers should differ by one rather than equaling half integers. However, this distinction is irrelevant in the thermodynamic limit, and thus the Hamiltonian becomes

$$\begin{aligned}\frac{H^Q_{\rm sgc2}}{k_BT} &= -\ln\left(\sum_{n_h=0}^{\infty}\sum_{n_c=0}^{\infty}\frac{(Q_{hA}Q_{hB})^{n_h/2}(zQ_c)^{n_c}}{[(n_h/2)!]^2 n_c!}\right) ,\\ &= -\ln\left(\sum_{n_h=0}^{\infty}\sum_{n_c=0}^{\infty}\frac{\left(2\sqrt{Q_{hA}Q_{hB}}\right)^{n_h}(zQ_c)^{n_c}}{n_h!n_c!}\right) ,\end{aligned} \tag{A4}$$

where we have used the approximation

$$[(n_h/2)!]^2 \approx \frac{n_h!}{2^{n_h}} . \tag{A5}$$

Ag with the grand canonical ensemble, the sums in Eq. (A4) are performed using the Taylor series of the exponential function, and from that Eq. (7) follows.

---

* Electronic address: r6spence@uwaterloo.ca

† Electronic address: mwmatsen@uwaterloo.ca

[1] K. R. Shull, E. J. Kramer, G. Hadziioannou and W. Tang, Macromolecules **23**, 4780 (1990).

[2] K. Chang, C. W. Macosko and D. C. Morse, Macromolecules **40**, 3819 (2007).

[3] D. Broseta and G. H. Fredrickson, J. Chem. Phys. **93**, 2927 (1990).

[4] L. Kielhorn and M .Muthukumar, J. Chem. Phys. **773**, 5588 (1997).

[5] A. Kudlay and S. Stepanow, Macromol. Theory Simul. **11**, 16 (2002).

[6] D. Zappalà, Phys. Lett. B **773**, 213 (2017).

[7] R. L. Scott, J. Chem. Phys. **17**, 279 (1949).

[8] H. P. Deutsch and K. Binder, Macromolecules **25**, 6214 (1992).

[9] T. M. Beardsley and M. W. Matsen, J. Chem. Phys. **147**, 044905 (2017).

[10] G. H. Fredrickson and E. Helfand, J. Chem. Phys. **87**, 697 (1987).

[11] J. Glaser, P. Medapuram, T. M. Beardsley, M. W. Matsen and D. C. Morse, Phys Rev. Lett. **113**, 068302 (2014).

[12] F. S. Bates, W. W. Maurer, T. P. Lodge, M. F. Schulz, M. W. Matsen, K. Almdal and K. Mortensen, Phys. Rev. Lett. **75**, 4429 (1995).

[13] Although the PE and PEP homopolymers in Refs. 12 and 15 have nearly equal polymerizations, they have much different invariant polymerizations indexes, $\bar{N}_{h,\mathrm{PE}} \approx 3000$ and $\bar{N}_{h,\mathrm{PEP}} \approx 10000$, due to the conformational asymmetry, $a_{\mathrm{PE}}/a_{\mathrm{PEP}} \approx 1.2$.

[14] G. Gompper and M. Schick, *Self-Assembling Amphiphilic Systems* (Academic Press, London, 1994).

[15] F. S. Bates, W. W. Maurer, P. M. Lipic, M. A. Hillmyer, K. Almdal, K. Mortensen, G. H. Fredrickson and T. P. Lodge, Phys. Rev. Lett. **79**, 849 (1997).

[16] D. Schwahn, K. Mortensen, H. Frielinghaus and K. Almdal, Phys. Rev. Lett. **82**, 5056 (1999).

[17] D. Schwahn, K. Mortensen, H. Frielinghaus, K. Almdal and L. Kielhorn, J. Chem. Phys. **112**, 5454 (2000).

[18] M. A. Hillmyer, W. W. Maurer, T. P. Lodge, F. S. Bates and K. Almdal, J. Phys. Chem. B

103, 4814 (1999).

[19] R. J. Hickey, T. M. Gillard, M. T. Irwin, D. C. Morse, T. P. Lodge and F. S. Bates, Macromolecules **49**, 7928 (2016).

[20] J. H. Lee, M. L. Ruegg, N. P. Balsara, Y. Zhu, S. P. Gido, R. Krishnamoorti and M.-H. Kim, Macromolecules **36**, 6537 (2003).

[21] V. Pipich, D. Schwahn and L. Willner, J. Chem. Phys. **123**, 124904 (2005).

[22] V. Pipich, L. Willner and D. Schwahn, J. Phys. Chem. B **112**, 16170 (2008).

[23] B. M. Habersberger, T. M. Gillard, R. J. Hickey, T. P. Lodge and F. S. Bates, ACS Macro Lett. **3**, 1041 (2014).

[24] M. Müller and M. Schick, J. Chem. Phys. **105**, 8885 (1996).

[25] J. Qin and D. C. Morse, J. Chem. Phys. **130**, 224902 (2009).

[26] D. Düchs, V. Ganesan, G. H. Fredrickson and F. Schmid, Macromolecules **36**, 9237 (2003).

[27] D. Düchs and F. Schmid, J. Chem. Phys. **121**, 2798 (2004).

[28] P. Stasiak and M. W. Matsen, Macromolecules 46, 8037 (2013).

[29] R. K. W. Spencer and M. W. Matsen, Macromolecules **49**, 6116 (2016).

[30] G. H. Fredrickson, V. Ganesan and F. Drolet, Macromolecules **35**, 16 (2002).

[31] G. H. Fredrickson, Soft Matter **3**, 1329 (2007).

[32] M. W. Matsen, J. Phys.: Condens. Matter **14**, R21 (2002).

[33] K. M. Hong and J. Noolandi, Macromolecules **14**, 727 (1981).

[34] M. W. Matsen, Phys. Rev. Lett. **74**, 4225 (1995).

[35] M. W. Matsen, Macromolecules **36**, 9647 (2003).

[36] M. W. Matsen, Euro. Phys. J. E **30**, 361 (2009).

[37] M. O. de la Cruz, S. F. Edwards and I. C. Sanchez, J. Chem. Phys. **89**, 1704 (1988).

[38] A. M. Ferrenberg and R. H. Swendsen, Phys. Rev. Lett. **61**, 2635 (1988).

[39] A. M. Ferrenberg and R. H. Swendsen, Phys. Rev. Lett. **63**, 1195 (1989).

[40] In Ref. 29, the expression for $\langle \hat{O} \rangle$ is missing the proper normalization constant, $\mathcal{N}$, but nevertheless the calculations were done correctly.

[41] K. Binder, Phys. Rev. Lett. **47**, 693 (1981).

[42] N. B. Wilding and P. Nielaba, Phys. Rev. E **53**, 926 (1996).

[43] E. M. Lennon, K. Katsov and G. H. Fredrickson, Phys. Rev. Lett. **101**, 138302 (2008).

[44] R. K. W. Spencer, B. Vorselaars and M. W. Matsen, Macromol. Theory Simul. **26**, 1700036

(2017).

[45] R. A. Riggleman and G. H. Fredrickson, J. Chem. Phys. **132**, 024104 (2010).

[46] M. Müller and F. Schmid, in *Advanced Computer Simulation Approaches for Soft Matter Sciences II*, edited by C. Holm and K. Binder (Springer-Verlag, Berlin, 2005).

[47] M. Sferrazza, C. Xiao, R. A. L. Jones, D. G. Bucknall, J. Webster and J. Penfold, Phys. Rev. Lett. **78**, 3693 (1997).

[48] R. A. Riggleman, R. Kumar and G. H. Fredrickson, J. Chem. Phys. **136**, 024903 (2012).

[49] Equation (22) for the interfacial tension, σ, is mathematically equivalent to that of Ref. 48, where tension is expressed in terms of the pressure normal and tangential to the interface.

[50] A. Werner, F. Schmid and M. Müller, J. Chem. Phys. **110**, 5370 (1999).

[51] P. Stasiak and M. W. Matsen, Eur. Phys. J. E **34**, 110 (2011).

[52] D. J. Audus, K. T. Delaney, H. D. Ceniceros and G. H. Fredrickson, Macromolecules **46**, 46 (2013).

[53] K. Chang, Ph. D. Thesis, University of Minnesota (2005).

[54] R. B. Thompson and M. W. Matsen, J. Chem. Phys. **112**, 6863 (2000).

[55] T. M. Beardsley and M. W. Matsen, Phys. Rev. Lett. **117**, 217801 (2016).

[56] M. Müller and K. Binder, Comp. Phys. Commun. **84**, 173 (1994).

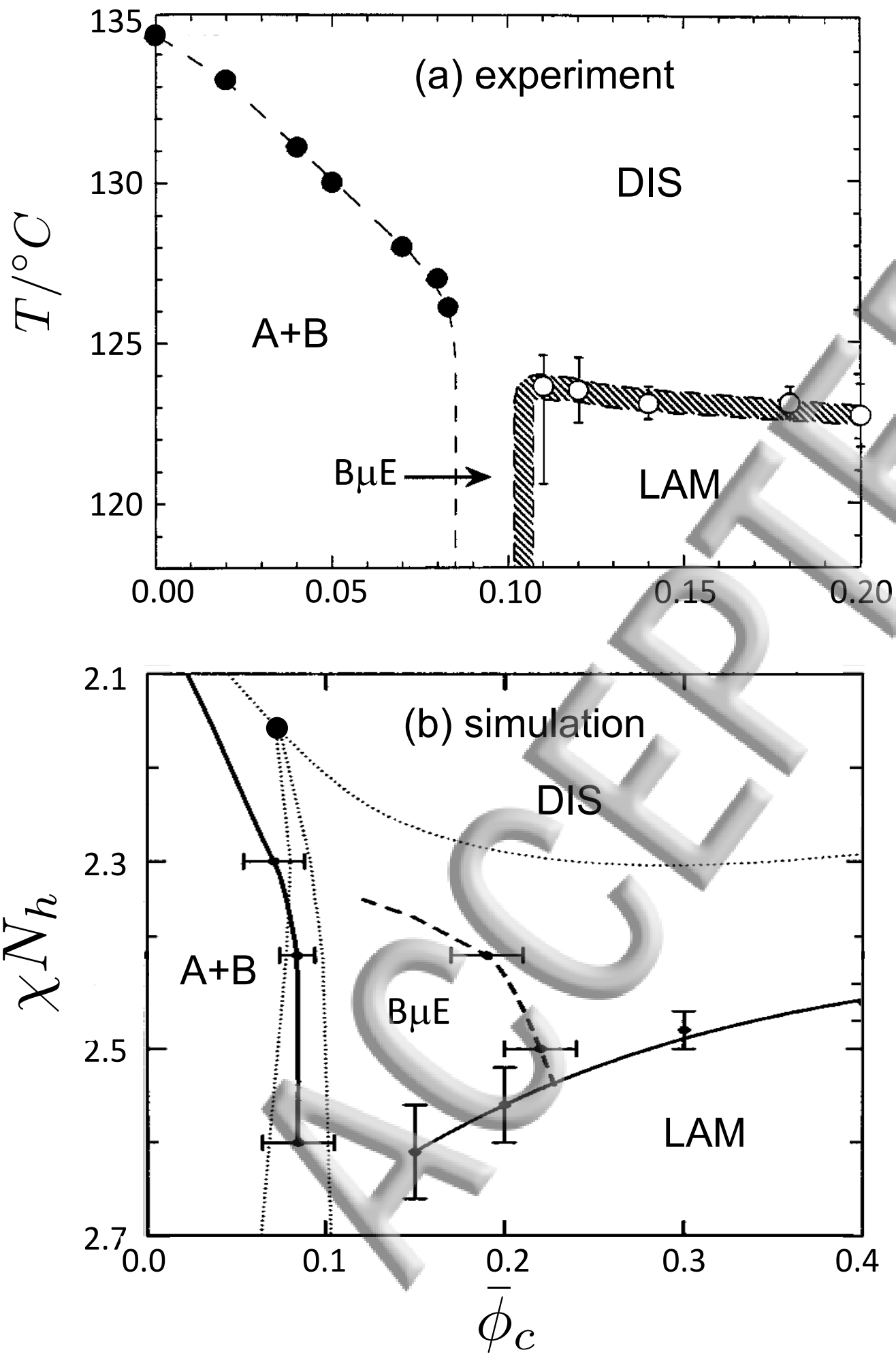
(a) experiment
DIS
A+B
BμE
LAM
$T/°C$
135
130
125
120
0.00
0.05
0.10
0.15
0.20
(b) simulation
DIS
A+B
BμE
LAM
χN_h
2.1
2.3
2.5
2.7
0.0
0.1
0.2
0.3
0.4
$\overline{\phi}_c$

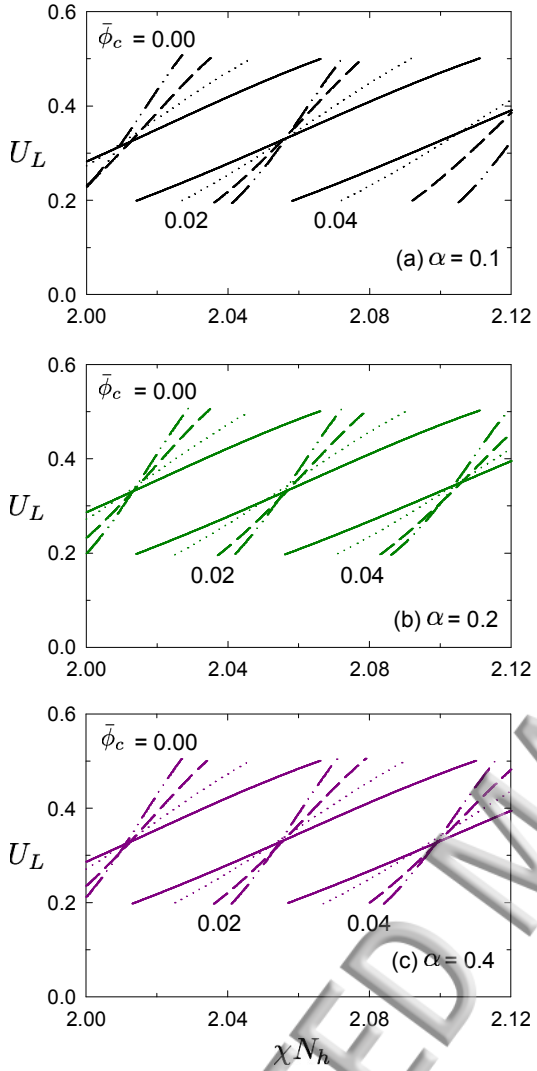
$\bar{\phi}_c$ = 0.00
0.02
0.04
(a) α = 0.1
(b) α = 0.2
(c) α = 0.4
U_L
χN_h
0.0
0.2
0.4
0.6
2.00
2.04
2.08
2.12

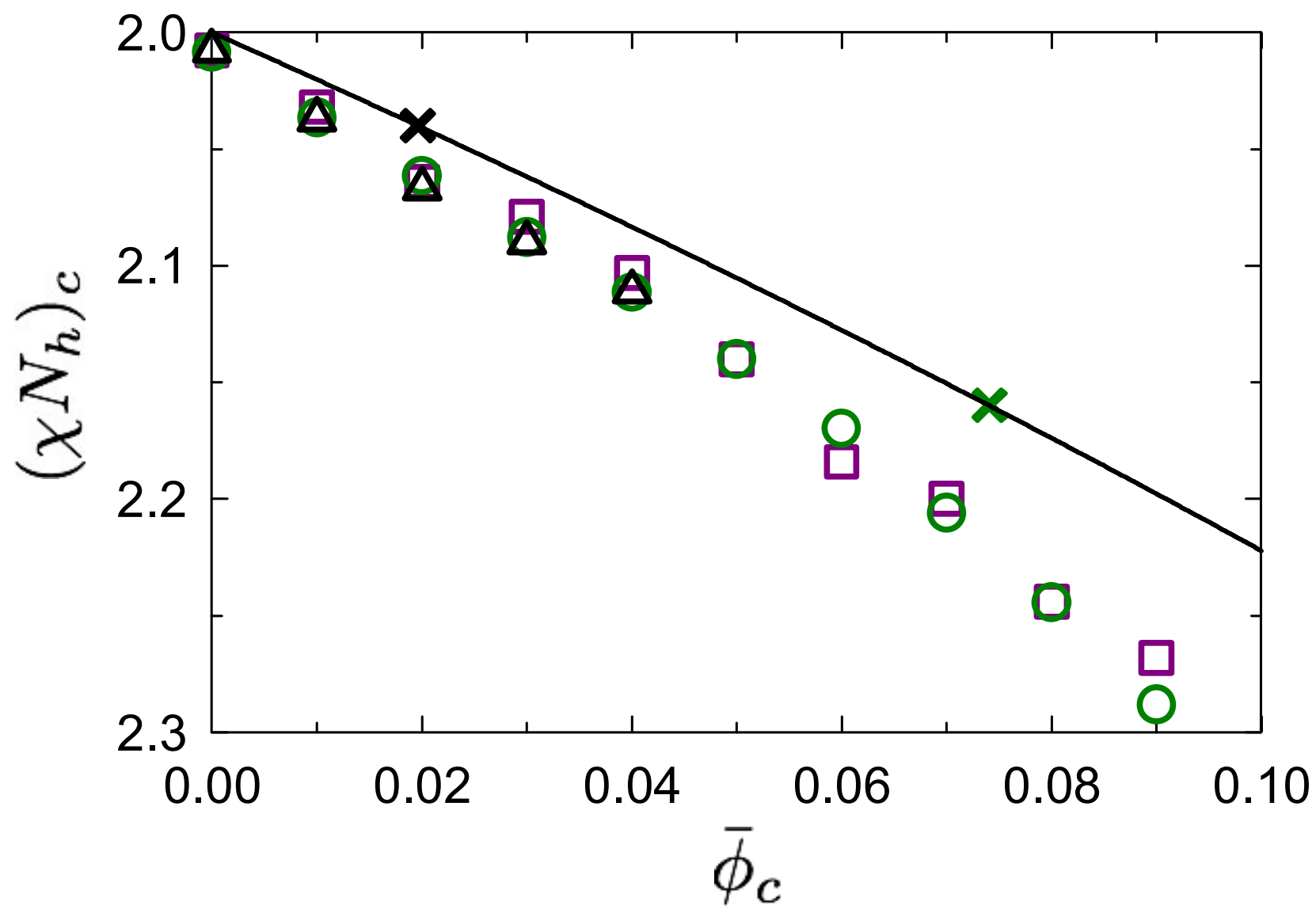
2.0
2.1
2.2
2.3
$(\chi N_h)_c$
0.00
0.02
0.04
0.06
0.08
0.10
$\bar{\phi}_c$

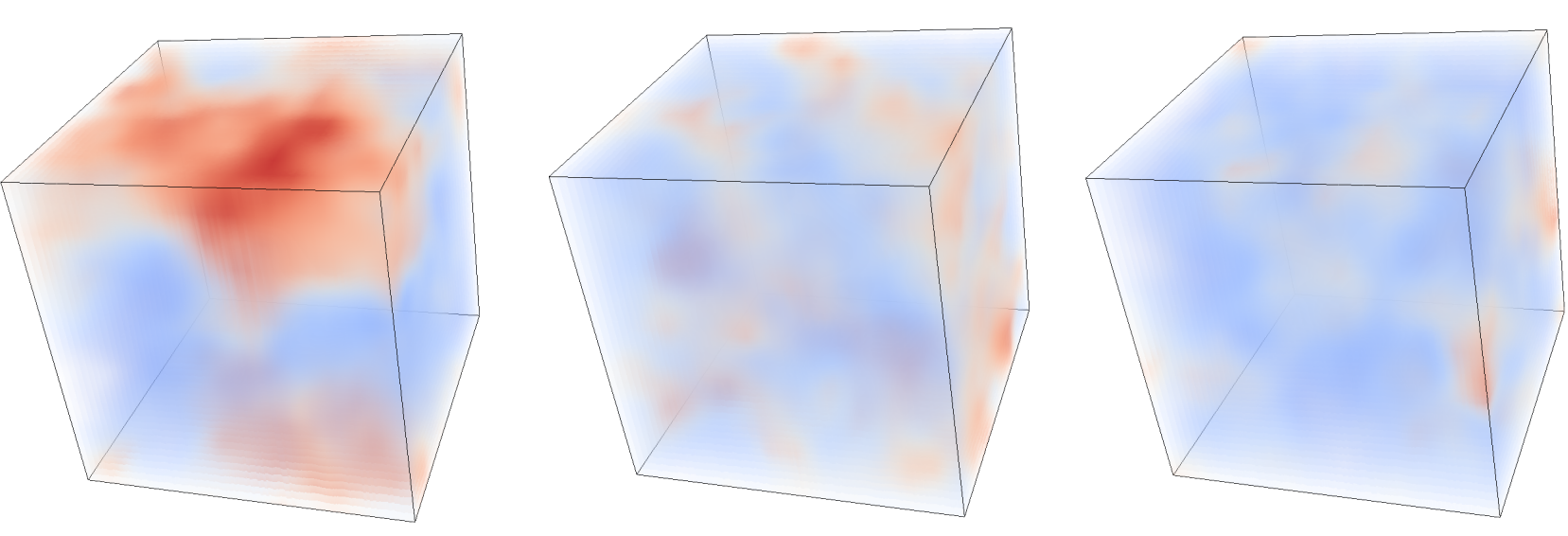

$(a)\,\alpha = 0.1$ $(b)\,\alpha = 0.2$ $(c)\,\alpha = 0.4$

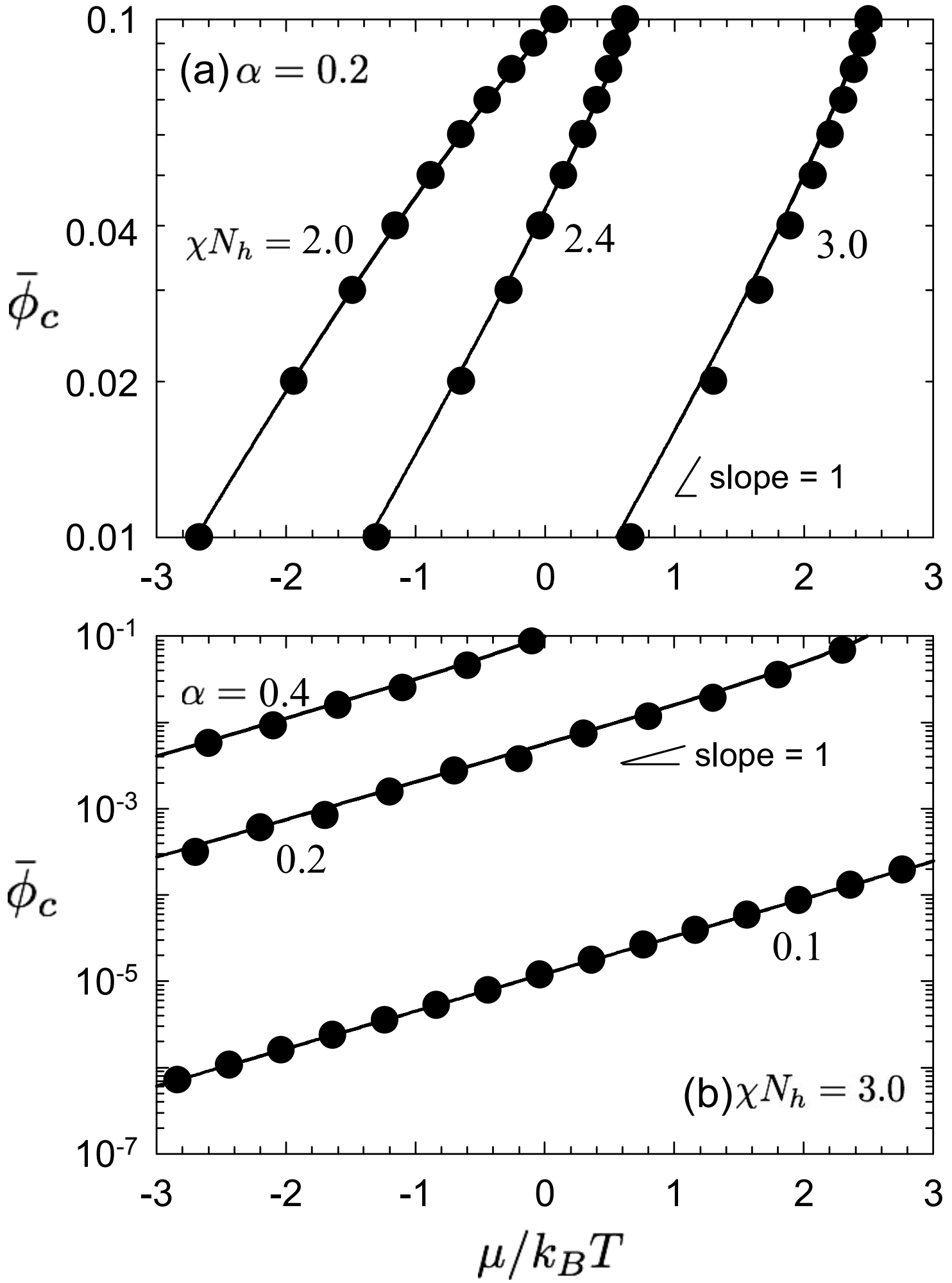
(a) $\alpha = 0.2$
$\chi N_h = 2.0$
2.4
3.0
slope = 1
$\bar{\phi}_c$
0.1
0.04
0.02
0.01
-3
-2
-1
0
1
2
3
$\alpha = 0.4$
slope = 1
0.2
0.1
(b) $\chi N_h = 3.0$
10^{-1}
10^{-3}
10^{-5}
10^{-7}
μ/k_BT

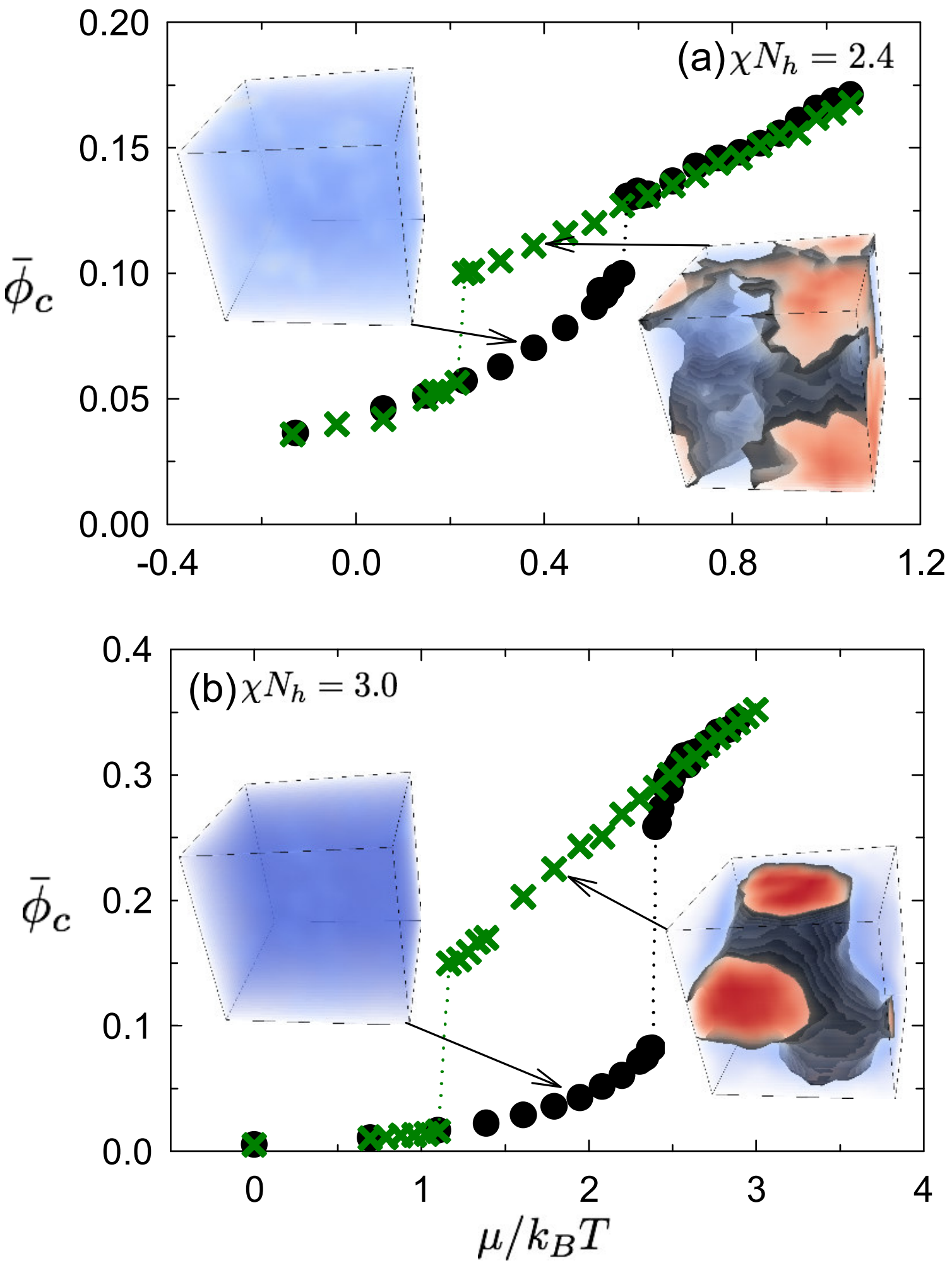
(a) $\chi N_h = 2.4$
$\bar{\phi}_c$
0.20
0.15
0.10
0.05
0.00
-0.4
0.0
0.4
0.8
1.2
(b) $\chi N_h = 3.0$
$\bar{\phi}_c$
0.4
0.3
0.2
0.1
0.0
0
1
2
3
4
μ/k_BT

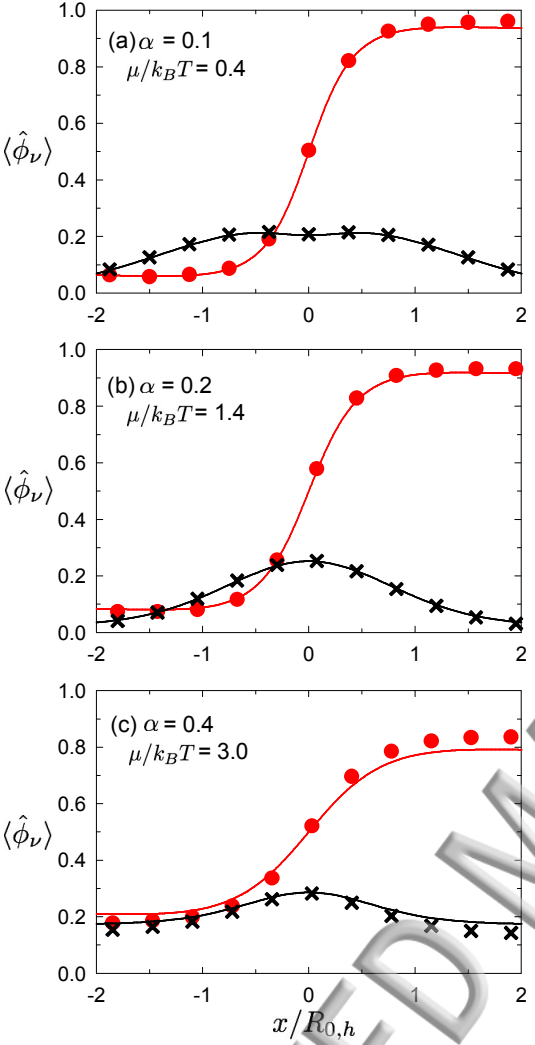
(a) α = 0.1
μ/k_BT = 0.4
(b) α = 0.2
μ/k_BT = 1.4
(c) α = 0.4
μ/k_BT = 3.0
$\langle\hat{\phi}_\nu\rangle$
$x/R_{0,h}$
0.0
0.2
0.4
0.6
0.8
1.0
-2
-1
0
1
2

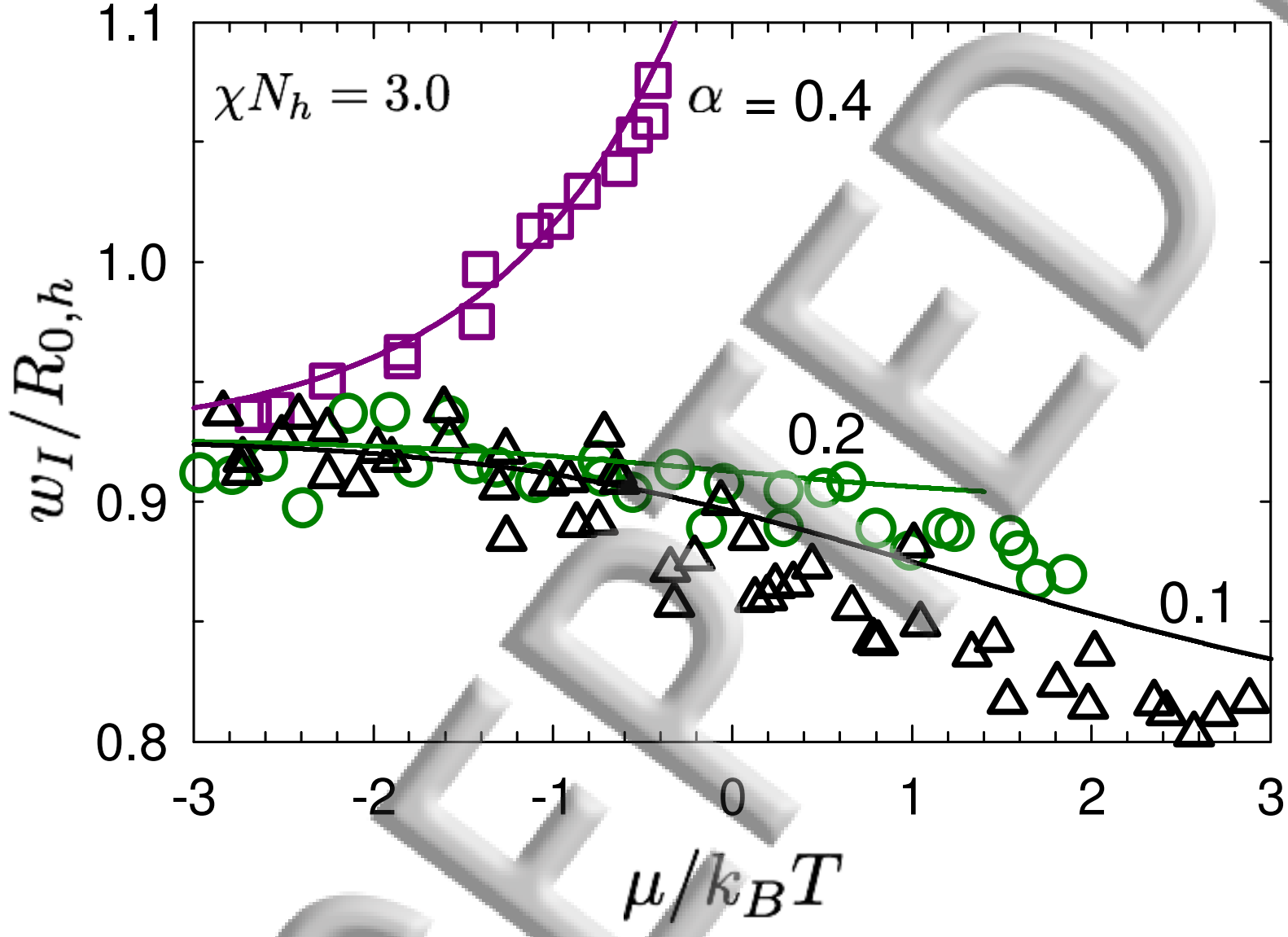
$\chi N_h = 3.0$
α = 0.4
0.2
0.1
$w_I / R_{0,h}$
$\mu / k_B T$
1.1
1.0
0.9
0.8
-3
-2
-1
0
1
2
3

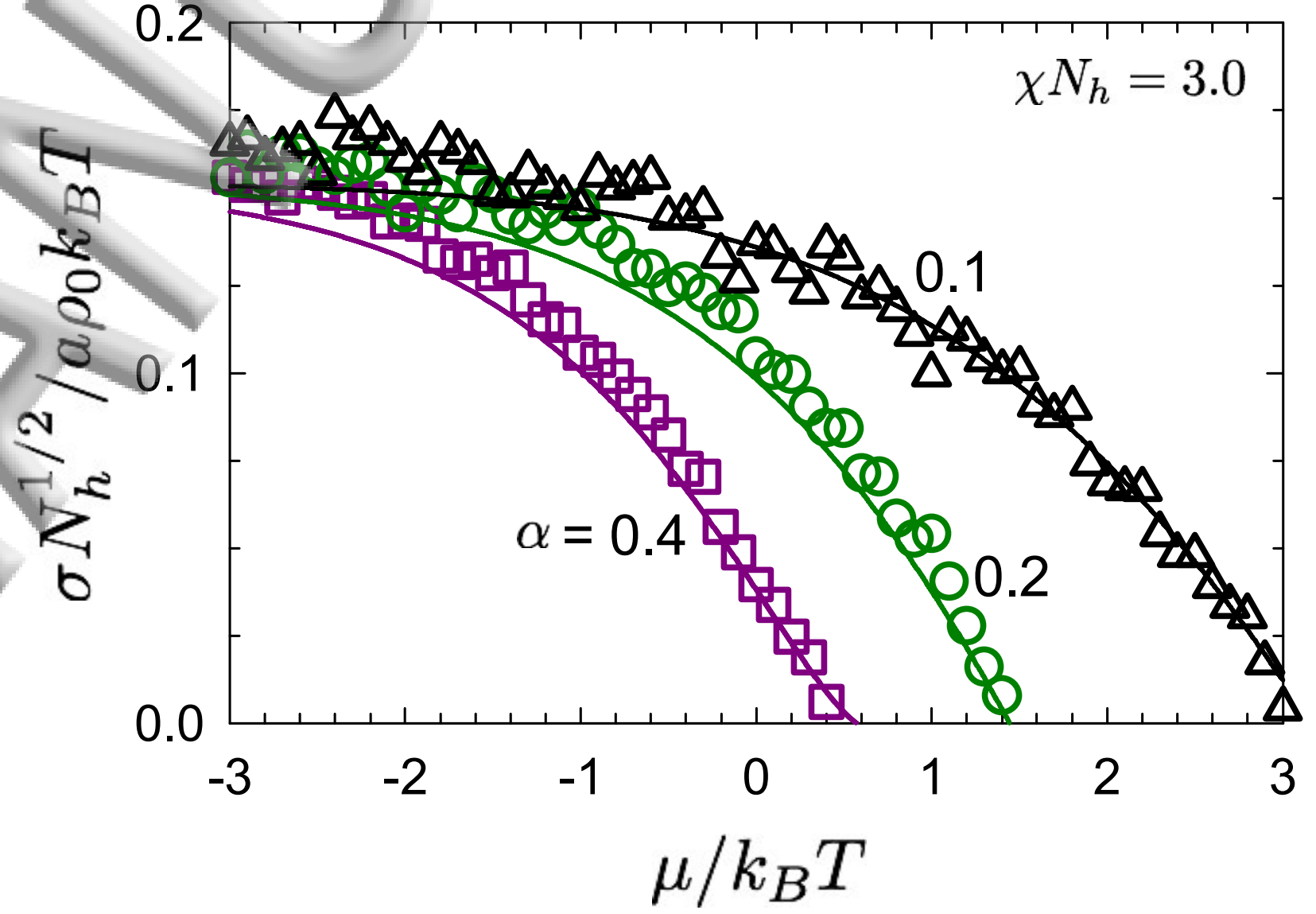
$\chi N_h = 3.0$
α = 0.4
0.1
0.2
$\sigma N_h^{1/2}/a\rho_0 k_B T$
$\mu/k_B T$
0.2
0.1
0.0
-3
-2
-1
0
1
2
3

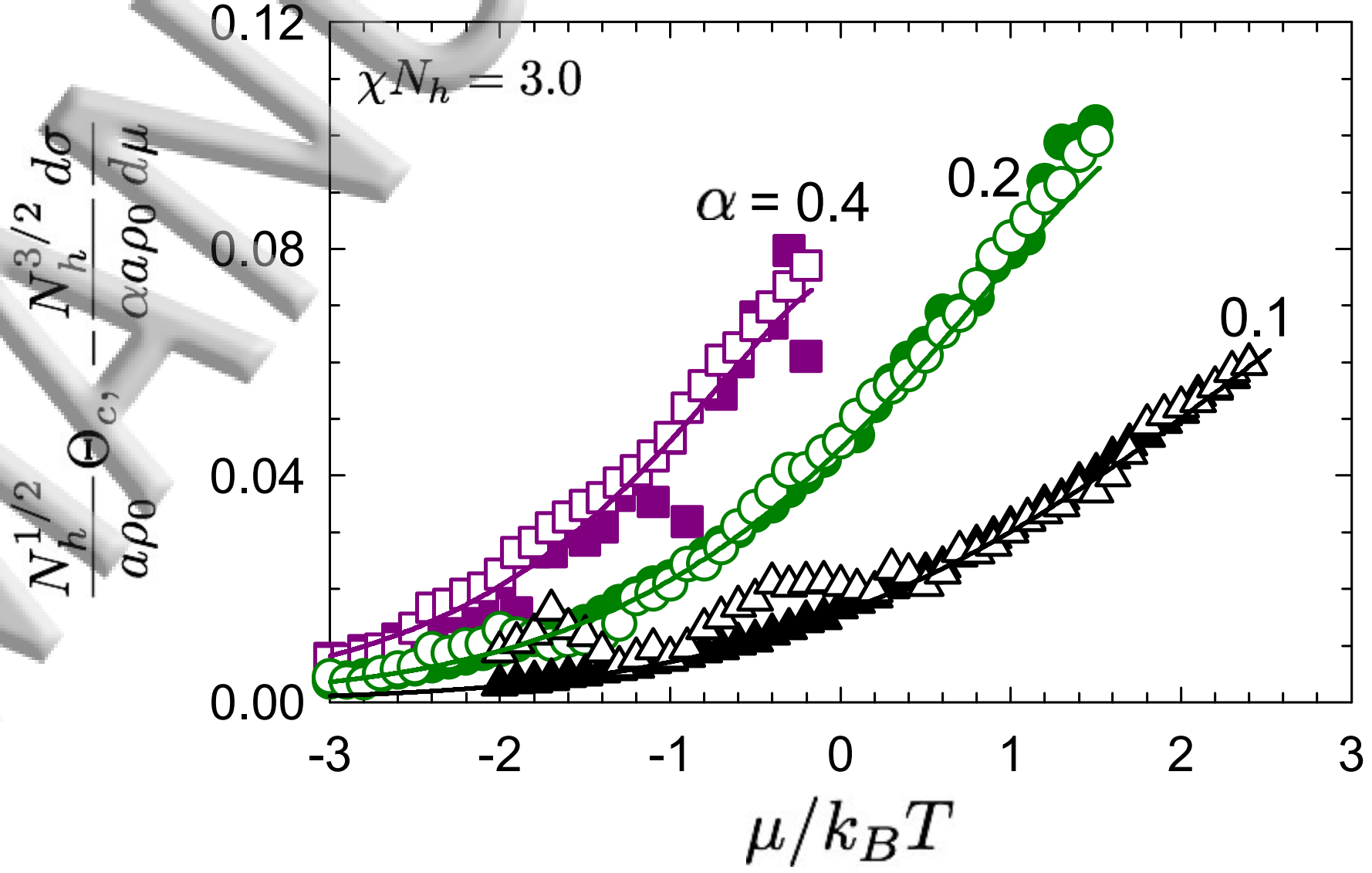
$\chi N_h = 3.0$
α = 0.4
0.2
0.1
0.12
0.08
0.04
0.00
-3
-2
-1
0
1
2
3
μ/k_BT
$\frac{N_h^{1/2}}{a\rho_0}\Theta_c, \frac{N_h^{3/2}}{\alpha a\rho_0}\frac{d\sigma}{d\mu}$